energy&fuels

Article

pubs.acs.org/EF

Ash Deposition Rates from Air and Oxy-Combustion of Pulverized Coal, Petroleum Coke, and Biomass

Yueming Wang, Xiaolong Li, and Jost O. L. Wendt*

Department of Chemical Engineering and Institute for Clean and Secure Energy, The University of Utah, 50 South Central Campus Drive, Salt Lake City, Utah 84112, United States

Supporting Information

ABSTRACT: This paper presents a synthesis of a large body of experimental data on growth rates of ash deposits from the air and oxy-combustion of multiple pulverized solid fuels, including coal, biomass, and their blends. The experimental data were obtained from 35 tests in a 100 kW (rated) entrained-flow combustor that allowed for self-sustained combustion of solid fuels. Ash deposition rates were measured using a wall-temperature-controlled ash deposition probe. The collected deposits were divided into tightly bound "inside deposits" adjacent to the heat transfer surface and loosely bound "outside deposits" that grow further out. Ash aerosol particle size distributions (psd's) and size-segregated compositions were obtained through electric mobility, light scattering, and impactor methods. Rates of ash deposition for both inside and outside deposits are presented. Rates of growth of the inside deposit were proportional to the sub-micrometer particle (PM_1) concentration in the flue gas but correlated poorly with the alkali concentration in the flue gas, while rates of growth of the outer deposits correlated poorly with PM_1 but well with the total alkali content in the flue gas. The data on growth rates of both types of deposits are interpreted in the light of available mechanisms. These involve a "glue effect" that was independent of composition of PM_1 for the inside deposits and a "bounce-off" criterion that depended upon the total alkali concentration in the flue gas for the outer deposits. These data from all 35 tests, burning 11 very different fuels, under similar (but not identical) aerodynamic conditions allow for prediction of changes in deposition rates of both inside and outside deposits as a result of changes in aerosol psd's and compositions. Data presented here may form the basis for future work leading to statistical models or mechanistic simulations of the ash deposition process.

1. INTRODUCTION

The effects of coal and biomass composition and combustion conditions on the mechanisms of ash formation have been widely investigated in numerous studies since the last century. However, extensive utilization of these solid fuel resources is still constrained by several challenges associated with emissions of SO_2, NO_x, and particulate matter (PM) and with other issues, such as slagging and fouling.[1−9] Ash deposition on the heat transfer surface is of interest because it reduces heat transfer efficiencies, causes corrosion of boiler surfaces, and even leads to costly boiler shutdowns.[1] Furthermore, the fouling propensity for oxy-combustion, with inlet oxygen concentrations of 30% (OXY30), has been observed to be higher than that for air combustion because of the lower particle velocity and the resulting longer residence time in the high-temperature zone under OXY30 conditions.[10] The focus of this paper is on gaining insight into what controls ash deposition rates for a wide range of solid fuels, including fossil fuels, biomass, and their blends, under both air and oxy-combustion conditions.

Deposition of the ash particles may occur by a number of different processes. These have been described in detail by Kleinhans et al.,[11] in their comprehensive review of ash particle sticking and rebound behavior. Typically, the larger particles are deposited by inertial impaction, including effects of eddy diffusion, while the smaller particles are deposited by thermophoresis or Brownian diffusion. In addition, uncooled vapors can condense or adsorb onto the wall surface directly.[3] An impacted particle may stick on the wall or rebound, where the sticking criteria are usually based on its viscosity, kinetic energy, and impaction angle.[11] The ash deposits thus formed can further capture additional incoming particles or be removed as a result of erosion by the flue gas.[12] These processes depend upon the particle and surface characteristics.

Ash deposits on a heat transfer surface can be mainly divided into two types:[13,14] (1) "inner" deposits (or inside deposits) that tightly adhere to the wall and can be removed only by scraping and (2) "outer" deposits (or outside deposits) that adhere loosely to the wall and can be easily removed by soot blowing. The formation of these two types of deposits most likely involves different mechanisms, leading to a smaller particle size in the inner deposits than in the outer deposits, as observed.[13] Because their deposit mass is dominated by the larger particles, the mass of the outer deposits is greater than that of the corresponding inner deposits.[15]

Although there exists copious literature on using numerical simulations[12,16−26] to predict ash deposition rates and characteristics for coal and biomass, most of these are valid only within narrow compositional ranges and do not differentiate between inner and outer deposits. The objective

Special Issue: 27th International Conference on Impact of Fuel Quality on Power Production and Environment

Received: December 2, 2018
Revised: January 31, 2019
Published: February 4, 2019

DOI: 10.1021/acs.energyfuels.8b04185
Energy Fuels XXXX, XXX, XXX−XXX

Table 1. Composition Analysis of 11 Solid Fuels

fuel	ash (%)	C (%)	H (%)	N (%)	S (%)	O (%)	H_2O (%)	volatile (%)	FC[a] (%)	HHV[b] (kJ/kg)
Sufco 1	8.36	67.87	4.77	1.09	0.36	11.44	6.11	38.49	47.04	27677
Sufco 2	13.96	62.41	4.52	1.10	0.46	11.04	6.52	37.36	42.16	27319
PRB	4.94	53.72	3.59	0.78	0.23	13.05	23.69	33.36	38.01	21115
Illinois	9.42	63.47	4.36	1.24	3.12	8.76	9.64	36.04	44.90	26870
PRB + Illinois	7.63	59.57	4.05	1.06	1.96	10.48	15.26	34.97	42.14	24568
rice husk	33.67	28.47	4.15	1.05	0.10	24.42	8.16	48.96	9.22	11551
husk + Sufco 1	13.42	59.99	4.67	1.08	0.31	14.04	6.52	40.58	39.48	24451
husk + PRB	8.67	50.44	3.66	0.82	0.21	14.53	21.67	35.39	34.27	19871
torrefied wood	0.19	51.75	5.29	0.14	0.02	36.29	6.32	74.2	19.29	21534
wood + Sufco 2	7.08	57.08	4.91	0.62	0.24	23.67	6.42	55.78	30.73	24427
petroleum coke	2.99	82.51	6.02	1.71	5.65	0.49	0.57	10.18	86.26	35720

[a]FC = fixed carbon. [b]HHV = higher heating value.

Table 2. Ash Analysis of 11 Solid Fuels

fuel	Al_2O_3 (%)	CaO (%)	Fe_2O_3 (%)	MgO (%)	MnO (%)	P_2O_5 (%)	K_2O (%)	SiO_2 (%)	Na_2O (%)	SO_3 (%)	TiO_2 (%)
Sufco 1	8.34	18.21	5.25	2.84	0.05	0.01	0.33	48.85	3.09	5.96	0.64
Sufco 2	12.09	11.90	3.62	3.94	0.03	0.25	1.13	62.48	0.81	1.83	0.68
PRB	14.78	22.19	5.20	5.17	0.01	1.07	0.35	30.46	1.94	8.83	1.30
Illinois	20.18	3.22	16.46	0.89	0.03	0.10	2.10	51.22	1.06	2.79	0.98
PRB + Illinois	18.02	10.81	11.96	2.60	0.02	0.49	1.40	42.92	1.41	5.21	1.11
rice husk	1.73	1.31	1.10	0.84	0.83	1.81	2.66	88.51	0.31	0.32	0.18
husk + Sufco 1	5.03	9.76	3.18	1.84	0.44	0.91	1.50	68.68	1.70	3.14	0.41
husk + PRB	8.26	11.75	3.15	3.01	0.42	1.44	1.51	59.49	1.13	4.58	0.74
torrefied wood	2.67	51.72	8.28	10.39	4.73	4.16	4.61	6.82	1.60	5.03	0
wood + Sufco 2	11.95	12.33	3.70	4.04	0.10	0.29	1.32	61.71	0.83	1.84	0.67
petroleum coke[a]	19.40	4.22	7.02	0.66	0.06	0.18	1.17	46.70	0.72	3.77	0.63

[a]For petroleum coke, there also exists 1.26% NiO and 8.24% V_2O_5 in ash other than the listed content.

of this work is to explore, through careful and systematic experimentation on a realistic 100 kW combustion test rig, commonalities in ash deposition mechanisms that predict growth rates of both inner and outer deposits for various fuels with a wide range of ash composition, which include coal, biomass, and their blends. Previous studies have reported the fouling deposition during air firing of coal and biomass blends,[17,27−31] but limited research is available for the deposition rates in oxy-fuel combustion.[32] Therefore, all of the fuels involved in this work are burned under air and oxy-combustion conditions.

It is commonly believed that the alkali content in the ash is the key factor for ash deposition on the wall, and considerable effort has been expended to determine the alkali metal partitioning during the combustion process and its effect on fouling.[33−37] Li et al.[38] suggested that fine particulates might have a "glue effect" for the ash deposits as a result of the high surface area/volume ratio and possible enrichment of the alkali content. However, other studies[39,40] have reported that these fine particulates are not necessarily rich in alkali content. This is because the vaporized alkali metal, such as sodium, can be increasingly scavenged by aluminosilicate particles, especially at high-temperature oxy-firing conditions, where inside deposition rates are higher.[15] Zhan et al.[15,41] developed a linear relationship between inner deposition rates and the sub-micrometer particle (PM_1) concentration for three coals that were burned in 16 different air- and oxy-combustion conditions,[15,41] despite the depletion of alkali metals in the PM_1 size range at some of the higher deposition rates. This relationship is extended to air and oxy-firing of rice husk.[42] This paper presents new additional data on inside deposit growth rates to further validate this relationship with 17 additional tests involving 8 solid fuels, including coal, biomass, and their blends. Furthermore, this paper greatly expands the database on measurements of growth rates of the loosely bound outer deposits for the tests referred to above. When added to the data available in the literature, the results provided here provide a comprehensive picture of how both inside and outside deposit growth rates depend upon ash aerosol particle size distributions (psd's), concentrations, and compositions and insight into mechanisms that appear to be valid for all solid fuels.

2. MATERIALS AND METHODS

2.1. Solid Fuel Properties. A total of 11 different pulverized solid fuels are investigated in this paper. These fuels include the following: (1) Powder River Basin sub-bituminous coal (PRB), (2) Illinois bituminous coal, (3) 40 wt % PRB/60 wt % Illinois blend (as originally envisaged for FutureGen 2.0[43]), (4) Utah Sufco coal 1, (5) Utah Sufco coal 2 (both being bituminous coals), (6) rice husks (supplemented by natural gas), (7) 20 wt % rice husk/80 wt % Sufco 1 blend, (8) 13 wt % rice husk/87 wt % PRB blend, (9) torrefied wood, (10) 50 wt % torrefied wood/50 wt % Sufco 2 blend, and (11) petroleum coke. Although partial results for fuels 1, 2, 3, and 6 have been published previously,[15,42,44] they are included here to provide a complete picture that, hopefully, allows for impacts of fuel quality on (near) universal mechanisms controlling ash deposition rates to be explored. Deposition rate data of the other seven fossil and biomass solid fuels are presented here for the first time, including one additional test for PRB burned in high-temperature oxy-combustion. These pulverized solid fuels have mean particle diameters from 70 to 200 μm. Their compositions and ash analyses can be found in Tables 1 and 2. Although Utah Sufco 1 and Utah Sufco 2 are from the same mine in Southern Utah, their ash contents are significantly different as

DOI: 10.1021/acs.energyfuels.8b04185
Energy Fuels XXXX, XXX, XXX−XXX

a result of the different seam involved as the source. Mass fractions of Na_2O and K_2O in ash are depicted (additively) in the bar chart in Figure 1. Biomasses tend to have larger amounts of K_2O than Na_2O

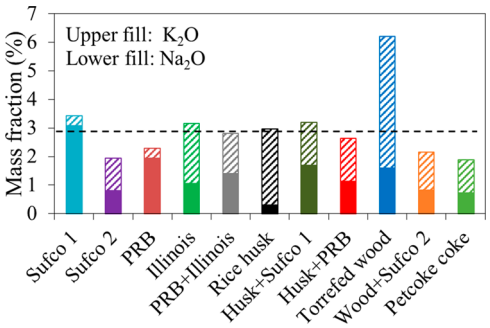

Figure 1. Mass fractions of Na_2O and K_2O in ash among these fuels.

because potassium is a key nutrient in biomass growth, while the relative content of Na_2O and K_2O varies throughout the different types of coal. However, it transpired that the sum of Na_2O and K_2O mass fractions in the ash for all of these diverse fuels, except the torrefied wood, lie within ±1.11% of the mean, 2.98% (Figure 1). Future work will expand the total alkali range, possibly through the use of additives.

To demonstrate the wide variations in how inorganic minerals were distributed among these fuels, the backscattered electron (BSE) microscope images of three selected solid fuels are shown in Figure 2: (a) torrefied wood, (b) petroleum coke, and (c) Sufco 1. The wood is in general a very clean feedstock; there are no excluded minerals detected; and most of the inorganic species are found embedded within the organic, regular wood matrix.[11] As a byproduct of the petroleum refining process, petroleum coke has a low ash content with some organically bound minerals and some excluded mineral grains or contaminants, such as soil or sand.[45] The coal generally contains excluded, included, and organically bound minerals, which are usually analyzed through computer-controlled scanning electron microscopy (CCSEM).[46] The point to be made is that the ash distributions are dramatically different among these fuels, and this is useful to explore universal ash deposition mechanisms among very varied initial forms of the mineral matter.

2.2. Combustion Conditions. All 11 fuels discussed in this paper were tested in air and oxy-combustion with an actual firing rate of ~27 kW, except that Sufco 2 was fired at 52 kW to achieve higher peak temperatures. It has been found that using recycled flue gas (RFG) with different cleanup options does not have a significant effect on ash transformation[47] and inside ash deposition rates, once the increased ash particle concentrations were taken into account. Hence, RFG was used only in the (already reported[47]) oxy-combustion of PRB, Illinois coal, and their blends. All other oxy-combustion cases reported here employ once through CO_2 to represent fully cleaned RFG. The oxy-combustion tests can be divided primarily into two categories: (1) using 27 vol % oxygen in the oxidant gas (denoted as OXY27), representing first-generation oxy-combustion processes with flame temperatures and heat fluxes similar to air firing, and (2) using 50 vol % oxygen in oxidant gas or higher (denoted as OXY50), representing advanced oxy-combustion with high flame temperatures and heat fluxes. The advanced oxy-combustion cases also include OXY70 and OXY80, in which all CO_2 was used to transport the fuel. For each case, the gas temepratures from ports 1 to 3 are measured by a ceramic-capped type B thermocouple, and the temperaures from ports 4 to 9 are measured by a unshielded type K thermocouple. The measured peak gas temperatures normally appear at port 2. The measured peak gas temperatures for air combustion and OXY27 are similar and usually 200−400 K lower than those in advanced oxy-combustion, depending upon the inlet O_2 percentage. Zhan et al. have reported that the changes in both the composition of PM and the inner layer of the deposits are attributed to the peak flame temperature, regardless of whether the dilution gas is N_2 or CO_2,[47] and this implies similar ash deposit properties between air combustion and OXY27. It should be mentioned that these fuels can be efficiently burned out before port 5 for air and oxy-firing conditions, and the carbon contents in collected deposits were generally lower than 3%. Petroleum coke is the only exception (with the carbon content in deposits higher than 25%) because of the extremely low volatile content and high fixed carbon, as shown in Table 1.

Table 3 summarizes test conditions for the 35 tests burning 11 solid fuels reported in this paper. Detailed operating conditions for selected cases can be found elsewhere,[15,39,42,47,48] and correspoding details of the others are not reported here for the sake of brevity. Some of the peak gas temperatures are not available, but one might reasonably estimate these temepratures by comparison to those measured for similar combustion coniditions. As shown in Table 3, different symbols are used to represent different cases, and similar cases use the same symbol for the sake of brevity. In summary, the ash deposition rates from all 11 fuels burned in air and oxy-combustion will be summarized to form a hypothesis to predict the ash deposition rates for a given fuel under certain combustion conditions.

2.3. Experimental Facilities. All of the experimental work discussed here was completed on a 100 kW (rated maximum) down-fired oxy-fuel combustor (OFC), which has been extensively used in previous studies for various pulverized solid fuels, including coal and biomass.[42,44,49,50] The OFC is a self-sustained (without external heating) and systematically controlled pilot-scale reactor; it operates at realistic stoichiometric ratios with turbulent diffusion flames in the ignition zone, resulting in realistic temperature/time profiles, although the flow becomes laminar downstream. The configuration of OFC is shown in Figure 3, and additional details about it can be found in ref

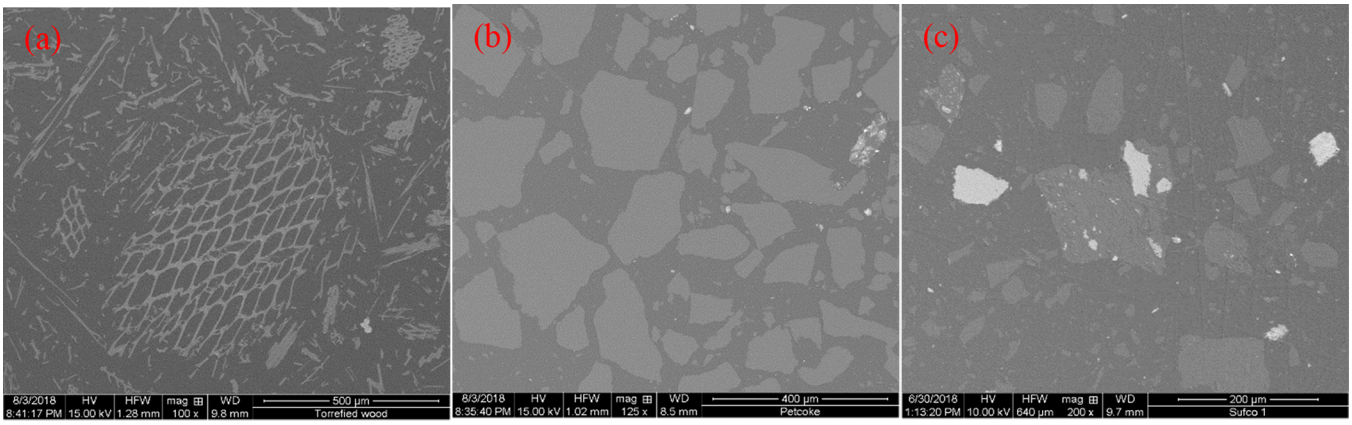

Figure 2. BSE images of three representative solid fuels embedded in carnauba wax: (a) torrefied wood, (b) petroleum coke, and (c) Sufco 1.

DOI: 10.1021/acs.energyfuels.8b04185
Energy Fuels XXXX, XXX, XXX−XXX

Table 3. Complete Tested Combustion Conditions

Fuel	#	Combustion condition	Abbr.	Firing rate (kW)	Peak gas temperature (K)	Flue gas rate (Nm^3/h)	Symbol
PRB	1	Air	P1	27	1347	33.0	□
	2	OXY27_once*	P2	27	1302	25.4	□
	3	OXY27_ash**	P3	27	-	25.4	□
	4	OXY27_ash/H_2O**	P4	27	-	25.4	□
	5	OXY27_ash/H_2O/S**	P5	27	-	25.4	□
	6	OXY27_dirty**	P6	27	-	25.4	□
	7	OXY50_once	P7	27	1508	14.4	■
	8	OXY50_ash	P8	27	-	14.4	■
	9	OXY50_ash/H_2O	P9	27	-	14.4	■
	10	OXY50_ash/H_2O/S	P10	27	-	14.4	■
	11	OXY80_once	P11	27	1583	9.9	■
Illinois	12	Air	I1	27	1360	31.1	□
	13	OXY27_ash	I2	27	1324	23.7	□
	14	OXY27_ash/H_2O/S	I3	27	-	23.7	□
40% PRB/60% Illinois	15	Air	PI1	27	1436	31.9	□
	16	OXY27_ash	PI2	27	-	24.1	□
	17	OXY27_ash/H_2O/S	PI3	27	-	24.1	□
Sufco 1	18	Air	$S_1$1	27	1455	31.7	□
	19	OXY27_once	$S_1$2	27	1414	24.1	□
	20	OXY70_once	$S_1$3	27	1689	9.6	■
Sufco 2	21	Air	$S_2$1	27	1350	28.9	□
	22	Air	$S_2$2	52	1489	57.1	▩
	23	OXY70_once	$S_2$3	52	1866	17.1	■
Rice Husks + N. Gas	24	Air	R1	33	1500	40.8	○
	25	OXY70_once	R2	33	1705	13.5	●
20% Rice Husks/ 80% Sufco 1	26	Air	$RS_1$1	27	1439	32.0	◇
	27	OXY70_once	$RS_1$2	27	1683	9.9	◆
13% Rice Husks/ 87% PRB	28	Air	RP1	27	1371	32.7	◇
	29	OXY70_once	RP2	27	1693	10.9	◆
Torrefied Wood	30	Air	T1	27	1325	30.1	○
	31	OXY70_once	T2	27	1751	10.0	●
50% Torrefied Wood/ 50% Sufco 2	32	Air	$TS_2$1	27	1281	30.0	◇
	33	OXY70_once	$TS_2$2	27	1711	9.4	◆
Petroleum Coke + N. Gas	34	Air	PC1	33	1324	40.5	△
	35	OXY70_once	PC2	33	1701	12.7	▲

*Oxy-combustion using pure CO_2 to simulate fully cleaned flue gas. **Oxy-combustion using flue gas recirculation with different cleanup options.

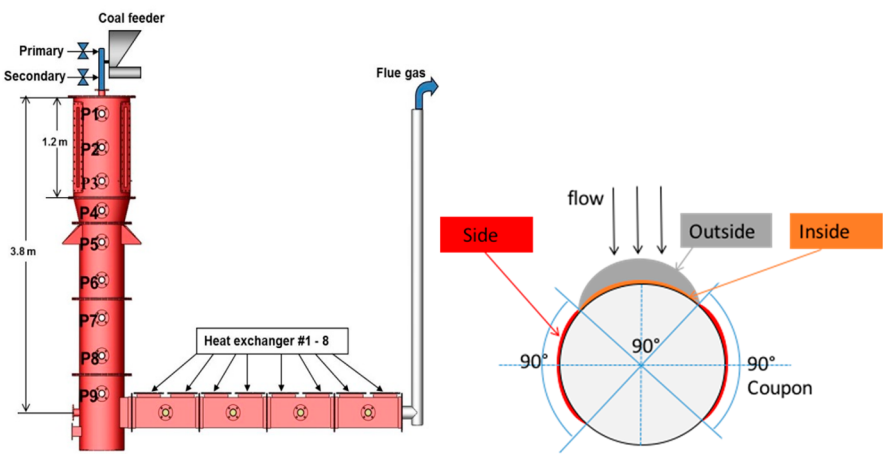

Figure 3. (Left) Configuration of OFC and (right) horizontal deposit division.[42]

42. Although the aerodynamics are significantly different from full-scale units, it is hoped that the deposition results generated from this test rig can be used to explore chemistry aspects of pertinent ash deposition mechanisms as they might occur in field units. Clearly, quantitative extrapolation of collection efficiencies to field units requires accurate simulations that account for effects of different

DOI: 10.1021/acs.energyfuels.8b04185
Energy Fuels XXXX, XXX, XXX−XXX

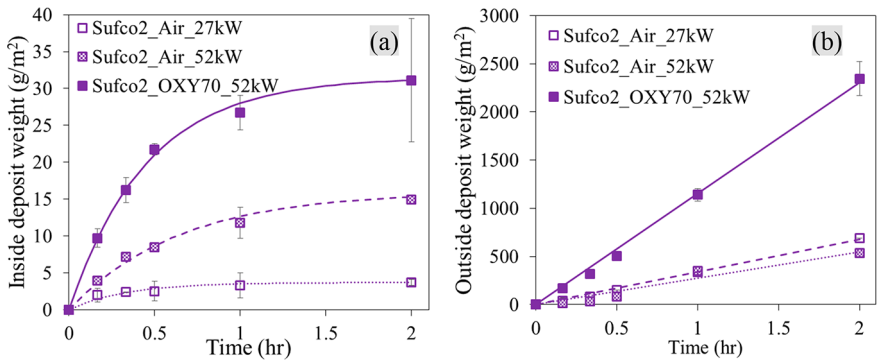

Figure 4. (a) Inside deposit weight and (b) outside deposit weight at various sampling times for Sufco 2 under different combustion conditions.

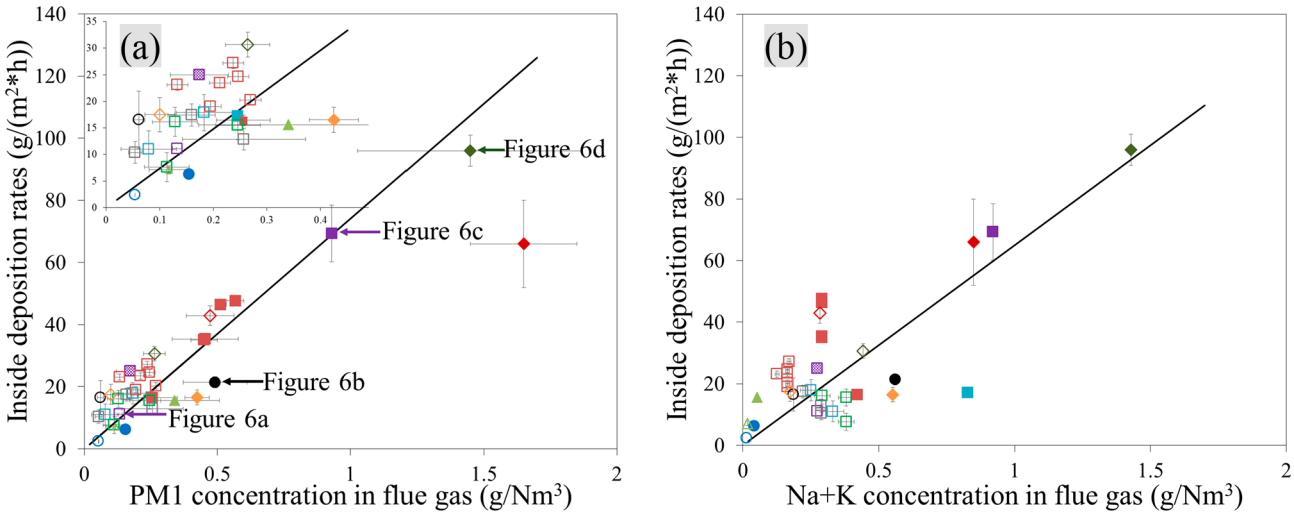

Figure 5. (a) Inside deposition rate correlation with the PM_1 concentration in the flue gas, $y = 74.06x$ ($r^2 = 0.71$), and (b) inside deposition rate correlation with sodium and potassium concentrations in the flue gas, $y = 64.93x$ ($r^2 = 0.47$).

aerodynamics, including turbulent deposition and the like. Therefore, results from this paper relate specifically to estimating differences in ash deposition rates as a result of differences in fuel composition and peak flame temperatures as they were achieved in this test rig.

In this work, ash deposits were collected by a air-cooled temperature-controlled deposit probe, which has been described in detail elsewhere.[13] Fouling ash is defined as the ash deposit on convective superheater tube surfaces that do not receive much radiation from the flame. The deposition probe was therefore inserted between ports 6 and 8 (see Figure 3), wherever the flue gas temperature was close to 1300 K. The wall temperature of the probe was controlled at 922 K, which is a typical surface temperature of the superheater in utility boilers. The collected ash deposits on the "coupon" can then be divided into side, inside, and outside deposits, as shown in Figure 3. This paper will focus on inside and outside deposits. In power plants, loosely bound fouling ash can be removed from the heat transfer surface by soot blowing, but a tightly bound deposit layer still remains. Therefore, the outside and inside deposits represent these loosely bound and tightly bound deposits, respectively. During the experiment work, the outside deposits were cautiously collected by rotating the probe and gently tapping it. The inside deposits remained stuck onto the probe and were collected by scraping the surface with a tool.

Ash aerosols were sampled through an isokinetic, water-cooled, and nitrogen-quenched dilution probe that is inserted in port 9, where the gas temperature was usually 1000 K. The flue gas temperature around the deposition probe is 300 K higher than the flue gas temperature at the aerosol probe (1300 K). HSC equilibrium calculations for PRB coal from the literature[51] and for Utah Sufco 1 coal shown in Figures S1 and S2 of the Supporting Information suggest that inorganic vapors have completely condensed after the flue gas temperature dropped below 1300 K, and little was changed for metal aerosols. The aerosol psd's were obtained using an online TSI scanning mobility particle sizer (SMPS, 0.0143−0.672 μm) and aerodynamic particle sizer (APS, 0.532−20 μm) combo. Size-segregated ash aerosol samples were collected on an 11-stage Berner low-pressure impactor (BLPI, 0.0324−15.7 μm), allowing elemental composition versus particle size distributions to be obtained using energy-dispersive X-ray spectroscopy (EDS). Additional details concerning the aerosol sampling and analysis technique can be found elsewhere.[39] A mass balance over the BLPI, including the pre-separator cup, was typically close to 70%. The BLPI plates alone collected less than 20% of the total ash. FEI Quanta 600 FEG SEM operated at 15 kV, coupled with an EDAX EDX system with a Si(Li) X-ray detector was used for the SEM/EDX measurements for ash aerosol and ash deposit.

2.4. Measurement of Growth Rates for Inside and Outside Deposits. To precisely determine the growth rate of inside and outside deposits, the ash deposits were collected at various sampling times ($^1/_6$, $^1/_3$, 0.5, 1, and 2 h), and then the weights of collected inside and outside deposits are separately plotted versus time. As noted above, the outside deposits were removed from the deposit probe by vigorous shaking, while the inside deposits required scraping for their removal and collection. Figure 4 shows the weight change of inside and outside deposits for Utah Sufco 2 under different combustion conditions (see Table 3). The error bars reflect the variations between measurements from at least three repeated tests, which imply that the measurement uncertainty for deposit weights is negligible. It is apparent here that the weight of the inside deposits increases rapidly at the beginning of the process and then stops growing after approximately 1 h. We believe this is because the inner

DOI: 10.1021/acs.energyfuels.8b04185
Energy Fuels XXXX, XXX, XXX−XXX

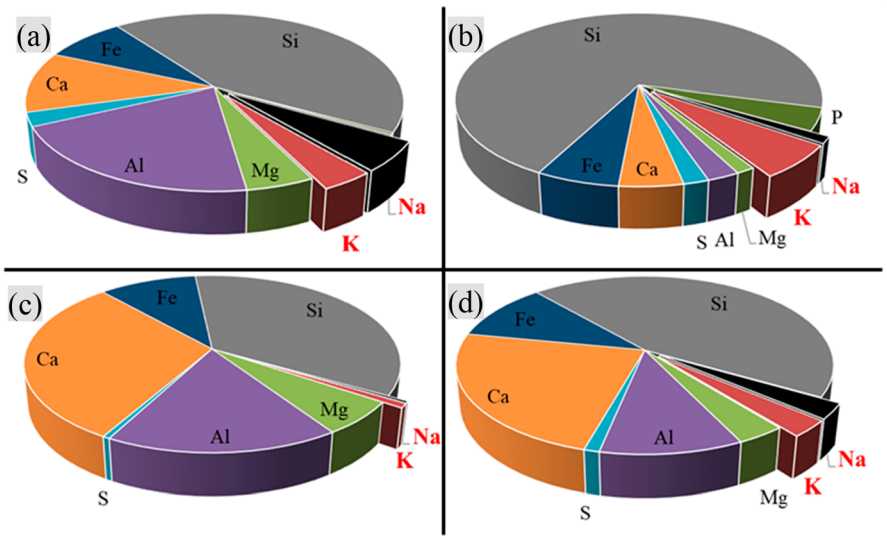

Figure 6. PM_1 composition analysis for different combustion conditions: (a) air of Sufco 2, (b) OXY70 of rice husk, (c) OXY70 of Sufco 2, and (d) OXY70 of 20% rice husk/80% Sufco 2.

layer is gradually isolated from the flue gas by the outer layer, which starts to take hold. We define the inside deposition rate as the initial growth rate, that is, the initial slope of the curve shown in Figure 4a. The weight of the outside deposit, on the other hand, increases at a constant rate continuously within a 2 h period. We believe this is because the outer layer is directly exposed to flue gas. For practical purposes, the outside deposition rate is thus defined as the average growth rate within a 2 h interval.

It should be noted that the weight of the inside deposit is significantly less than that of the outside deposit at the same sampling time. In other words, one can neglect the mass of inside deposits if the deposits are collected together and considered as a whole, and the total weight is all that one is interested in. Figure 4 shows deposition rate behavior that is typical of the other solid fuels examined here. It should be noted that the particle rebound can significantly affect the weights of ash deposits,[11] but this is a complex phenomenon and is discussed within the context of the results obtained here in the Discussion below.

3. RESULTS

3.1. Inside Deposits. In this section, deposition rates are presented here for inside deposits for all of the 35 cases noted in Table 3. It has been discussed that PM_1, of any composition, might have a "glue effect" on ash deposition formation,[38] forming the inside layer. Zhan et al.[15] discovered a linear relationship between the inside deposition rates and the PM_1 concentration in the flue gas, in contrast to the alkali content of PM_1. To further validate this hypothesis, the experimental results from an additional eight solid fuels in air and oxy-combustion were added to yield an expanded correlation between inside deposition rates and the PM_1 concentration in the flue gas, as shown in Figure 5a. This figure includes published results[15,42] and new results. It should be noted that all of the PM_1 concentrations were measured using BLPI and the measurement of each case was repeated at least 3 times to limit the uncertainty.

It has been long believed that the alkalis alone are the "bad actors" controlling ash deposition. Therefore, the measured inside deposition rates are also plotted against the total alkali metal concentration in the flue gas (Figure 5b). Symbols denote the different fuels and conditions as in Table 3. The correlation of the inside deposition rate with the alkali metal concentration in the flue gas is poor (R^2 = 0.47). The alkali metal concentrations on the horizontal axis of Figure 5b include Na and K contained within a wide range of species, namely, sulfates, chlorides, or aluminosilicates. These concentrations are calculated from the feed rate of Na and K (g/h) divided by the flue gas flow rates (Nm^3/h). It should be noted that the calculated alkali metal concentrations might differ with the actual values because of potential losses as a result of deposition on the combustor and sample line surfaces. *In situ* measurements of alkali metal will be considered in future work.

Figure 5a, however, is important, because it clearly shows that the inside deposition rates are indeed proportional to the PM_1 concentration in the flue gas over a wide range of fuels and combustion conditions. The R^2 correlation coefficient is 0.71 considering all of the data without exception. If the single outlier red solid filled symbol, denoting case 29 (OXY70 for 13% rice husk/87% PRB blend), is omitted from the correlation, the correlation coefficient increases to a R^2 = 0.83. It should also be noted that PM_1 concentrations are significantly higher for high flame temperatures (i.e., for oxy-combustion, denoted by symbols with a solid fill) compared to those at lower flame temperatures (i.e., for air- and temperature-modulated oxy-combustion, denoted by open symbols) for the same fuel, and effects of this are discussed below.

Panels a−d of Figure 6 depict the measured PM_1 composition for sample particles denoted accordingly on Figure 5a. These four samples all fall close to the linear correlation, yet they have widely different compositions. Indeed, the sample shown on Figure 6c is essentially devoid of alakli metals but has a high inside deposition rate, while the sample with the highest alkali metal content (Figure 6a) has the lowest inside deposition rate. Clearly, it is not the alakli metal content of PM_1 that controls the inside deposition rate but only the presence of PM_1 of any composition. Note again that, generally, the highest inside deposition rates occur at the greatest PM_1 concentrations in the flue gas, which tend to occur under combustion conditions that yield the highest peak flame temperatures, namely, at the highest firing rates (52 kW) and highest oxygen enrichments (OXY70).

3.2. Outside Deposits. Following the method of presenting results for the inside deposits, deposition rate data

DOI: 10.1021/acs.energyfuels.8b04185
Energy Fuels XXXX, XXX, XXX−XXX

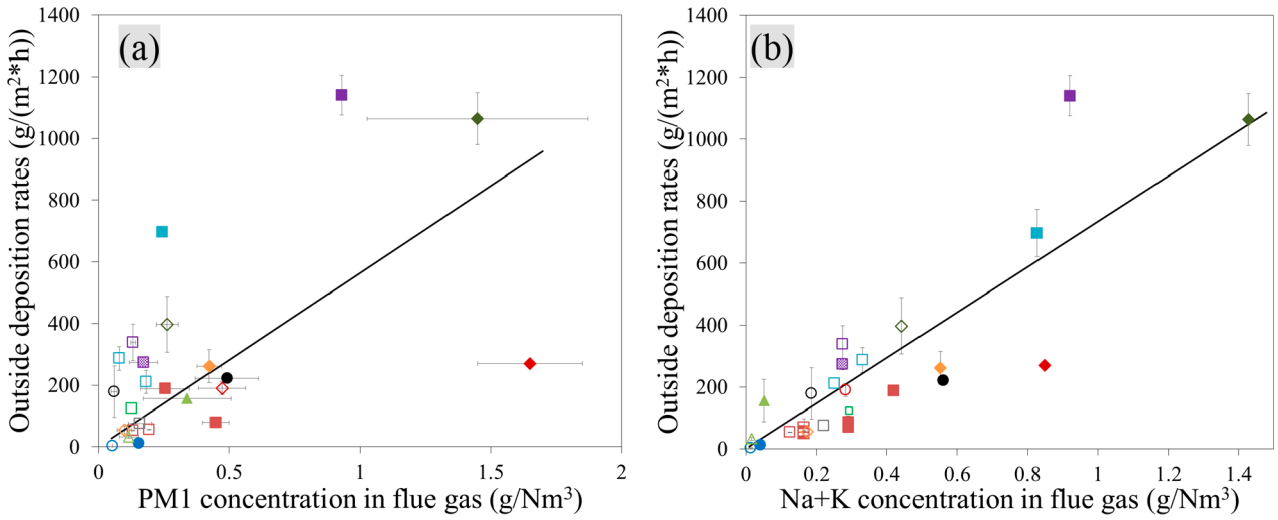

Figure 7. (a) Outside deposition rate correlation with the PM_1 concentration in the flue gas, $y = 563.5x$ ($r^2 = 0.27$), and (b) outside deposition rate correlation with sodium and potassium concentrations in the flue gas, $y = 733.25x$ ($r^2 = 0.75$).

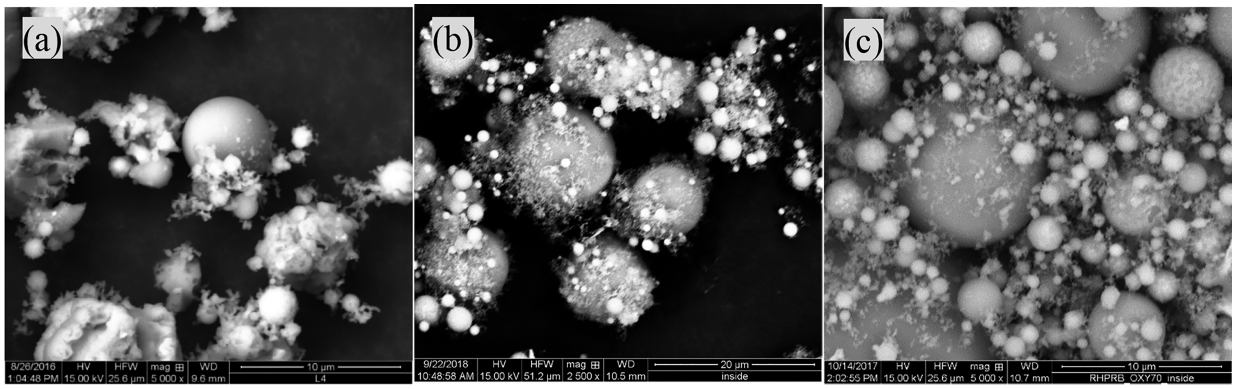

Figure 8. BSE images of inside deposits from some selected cases: (a) OXY70 of Sufco 1, (b) OXY70 of Sufco 2, and (c) OXY70 of 13% rice husk/87% PRB.

for the outside deposits are reported here using similar correlations. As for the inside deposit rate data, Figure 7a shows the outside deposition rate plotted against PM_1, while Figure 7b shows the same quantity versus the total alkali content in the flue gas. The results are the converse of those for the inside deposits. Now, for the outside deposits, the deposition rate does correlate with the total alkali content in the flue gas, while that versus PM_1 does not. Clearly, PM_1, which was purported to be the controlling sticking parameter for the inside deposition rate, does not fill that role for the outside deposition rate. The scatter for outside deposition rates in Figure 7b, is considered to be acceptable to make this correlation, because the deposits were loosely bound and were therefore more likely to be missed in the weight measurement.

It should be noted that outside deposition rates are very much larger than those for the inside deposits. The measured range for the outside deposition rate is from 0 to 1200 g m^{-2} h^{-1}, while that for the inside deposition rate is from 0 to 100 g m^{-2} h^{-1}. It should also be noted that the correlation shown on Figure 7a with an abscissa of the Na + K concentration in the flue gas, with a correlation coefficient ($r^2 = 0.75$), is essentially interchangeable with the correlation between outside deposition rates and total ash concentration in the flue gas ($R^2 = 0.774$), which is not surprising, given that the Na + K concentration in the ash was (by chance) approximately constant for all of the fuels (see Figure 1).

4. DISCUSSION

4.1. Inside Deposits. Figures 5 and 6 suggest that the deposition rates of inside deposits are controlled by the presence of PM_1 of any composition and that high inside deposition rates can result from many particles with extremely low alkali metal contents. Alkali metals, indeed, are less pronounced in PM_1 at the higher flame temperatures (see Figure 5) because higher peak temperatures accelerate the scavenging of alkali metal vapor by larger aluminosilicate particles.[40] Although the bulk of the mass of the inside deposits is contained in the larger particles in the deposit, one might speculate that the rate at which these larger particles adhere to the bare tube is controlled by the "glue effect" of PM_1, of any composition. To further "visualize" the glue effect of PM_1 for inside deposit formation, backscattered electron (BSE) images of inside deposits are shown in Figure 8 for (a) OXY70 for Sufco 1, (b) air for Sufco 2, and (c) OXY70 for the 13% rice husk/87% PRB blend. These pictures suggest that PM_1 indeed tends to stick on the surface of large particles or agglomerate together to form clusters. We attempted to correlate the inside deposition rates with other parameters, but none of those correlated with R^2 values close to 0.71, the value in Figure 5a.

DOI: 10.1021/acs.energyfuels.8b04185
Energy Fuels XXXX, XXX, XXX−XXX

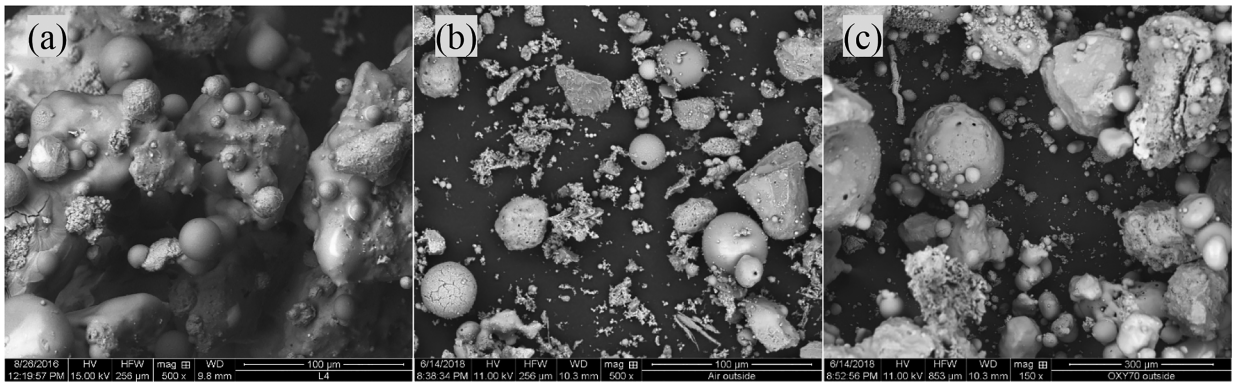

Figure 9. BSE images of outside deposits from some selected cases: (a) OXY70 of Sufco 1, (b) air of Sufco 2 (52 kW), and (c) OXY70 of Sufco 2.

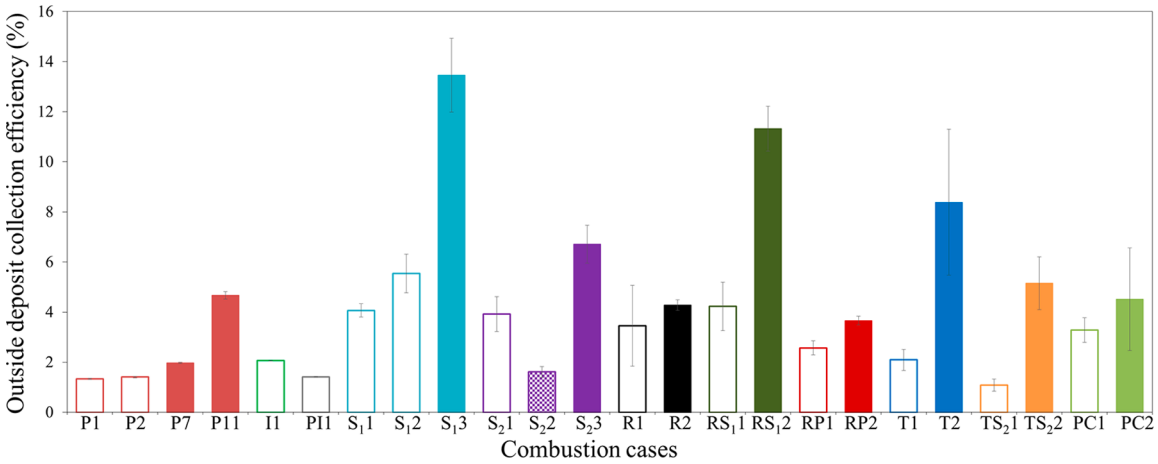

Figure 10. Outside deposit collection efficiencies for selected combustion cases. See Table 3 for the abbreviations used in the abscissa designating cases.

One might further speculate that the adhesion probability of PM_1 can be high as a result of their low kinetic energies.[11] In contrast to this, the super-micrometer particles with a much higher kinetic energy can easily bounce off the coupon surface. After the formation of the powdery layer of PM_1 on the wall, the super-micometer particles can be glued by deposited PM_1. Therefore, PM_1 can promote and control the formation of the (tight) inside deposits.

The results here supplement the work of Li et al.,[38] who studied the properties of ash aerosol and ash deposition in Zhundong lignite, which is rich in alkali and alkali earth metal (AAEM). There, PM_1 was enriched in alkali species, such as sodium sulfate and soidum chloride, which have low melting points. Li et al. hypothesized that this sticky and alkali-rich PM_1 could work as a "glue" to capture larger particles. However, the work presented here confirms previous suggestions[39,40] that PM_1 does not need to be enriched in alkali to be effective as "glue", at least as far as the tight inside deposits are concerned.

4.2. Outside Deposits. The deposition rate of the outside deposits is over 10 times that of the inside deposits. Furthermore, the inside deposition rate diminishes with time (Figure 4a), while the outside deposition rate is approximately constant (Figure 4b). It appears that the formation of these two types of deposits involves different mechanisms. At the beginning, the small particles driven by a combination of inertial impaction and thermophoresis can impact and deposit on the smooth surface, but the incoming large particles are not retained on the smooth surface as a result of their high kinetic energy. They bounce off. After the inside deposit is formed, the temperature gradient between flue gas and the coupon surface decreases as a result of the low thermal conductivity of the ash deposit. At that point, the thermophoresis driving force is diminished. The large particles, on the other hand, can now be deposited because the kinetic energy can be absorbed by the powdery inner deposit layer. According to this hypothesis, (a) the inner deposits will be enriched in small particles, (b) the rate of increase of the inside deposits will diminish with time, and (c) the weight of outer deposits will be significantly higher than that of the inner deposits. All of these phenomena have been observed in this work.

One might expect inertial impaction to be the dominant rate-controlling process for outside deposits. Figure 9 shows the BSE images of outside deposits for several cases. Panels a and c of Figure 9 indicate that there exists severe ash sintering for outside deposits because they are directly exposed to the hot flue gas. In contrast to the inside deposits, no clear adhesion of PM_1 (or PM_1 glue effect) can be seen on these large particles, and this is consistent with the lack of correlation on Figure 7a.

The data on Figure 7b deserve further discussion. Close examination reveals that, for the same fuel, higher (outside) deposition rates were observed under lower flue gas velocities, such as occurred for OXY70. In view of the fact that one might expect decreased impaction rates at lower flue gas velocities, the data suggest that it is particle bounce-off that controls the

DOI: 10.1021/acs.energyfuels.8b04185
Energy Fuels XXXX, XXX, XXX−XXX

outside deposition rate. Particles impacting at lower velocities have lower kinetic energy to be dissipated, following the approach of Zhou et al.[25] To explore this further, it is useful to compare, for each run, the overall collection efficiency (η), which combines aerodynamic effects, causing impaction, with chemical effects causing sticking. It is defined as the ratio of the rate per unit surface area at which PM adheres to the surface (g m^{-2} h^{-1}) to the mass flux of PM flowing through the same projected area in the flue gas (i.e., without a disturbance caused by the surface, g m^{-2} h^{-1}) and is calculated as

$$\eta = \frac{r_{\text{deposit}}}{f_{\text{fuel}} w_{\text{ash}} / A_{\text{OFC}}} \times 100\%$$

where r_{deposit} is the outside deposition rate on the coupon (g m^{-2} h^{-1}), f_{fuel} is the fuel feeding rate (g/h), w_{ash} is the ash content in the fuel (%), and A_{OFC} is the cross-section area of the reactor at port 6 (m^2). Results are shown on Figure 10 using the same color coding as in all of the tables and figures shown above, and from this figure, one might deduce the following: (1) For the same fuel, cases with higher velocity have a lower collection efficiency, even though the impaction efficiency is higher. For example, the average gas velocity for Sufco 1 at the sampling port of cases 18, 19, and 20 is 0.746, 0.661, and 0.254 m/s, respectively, with the collection efficiency for each of these three cases being 4.07, 5.54, and 13.46%, respectively. Additionally, the high peak gas temperature in case 20 also contributes to the high collection efficiency because it is reported that the particle sticking probability is more likely to be affected by the maximum experienced temperature rather than the local temperature.[26] (2) The overall collection efficiencies for all of these fuels are relatively low and typically around 2−14% for most cases because of the relatively low particle Stokes numbers (all much less than 1). The highest collection efficiencies were seen for Sufco 1 OXY70 (case 20), 20% rice husk/80% Sufco 1 blend at OXY70 (case 27), and torrefied wood at OXY70 (case 31), all of which had among the lowest flue gas flow rate and highest peak gas temperature. (3) Although outside deposition rates of torrefied wood and petroleum coke are an order of magnitude lower than those of other fuels, as shown in Figure 7, their collection efficiencies are about the same level.

5. CONCLUSION

A large body of experimental data of ash deposition rates was obtained from the air and oxy-combustion of 11 solid fuels (coal, biomass, and their blends) that were burned in 35 tests in a self-sustained entrained-flow combustion rig. Deposition rates were divided into those for the inside, tightly bound layer and those for the looser, outside deposit layer that can be more easily removed by soot blowing. The significant differences in ash compositions among these 11 fuels can be used to explore deposition mechanisms common to all fuels. Although aerodynamic factors clearly influence ash deposition rates in practical systems, this work does suggest that changes in inside and outside deposition rates can be estimated by knowledge of the ash aerosol characteristics. These characteristics are, for inside deposits, the concentration of PM_1, which can be measured online in real time using existing instrumentation, and, for outside deposits, the concentration of total alkali in the ash aerosol, which can be calculated or at least estimated. Inside deposition rates do not depend upon the alkali content of the particles making up the deposit. Outside deposits are primarily formed by inertial impaction, and the data here suggest that collection efficiency increases with decreasing flue gas velocity, most likely because of changes in particle bounce-off behavior.

■ ASSOCIATED CONTENT

Supporting Information

The Supporting Information is available free of charge on the ACS Publications website at DOI: 10.1021/acs.energyfuels.8b04185.

Detailed, full size image of the inset of Figure 5a, showing the lower end of the inside deposition rate correlation with the PM_1 concentration in the flue gas (Figure S1), HSC equilibrium calculation of the mineral species containing Na, Mg, K, Ca, and Fe for air combustion of Utah Sufco 1 (Figure S2), and HSC equilibrium calculation of the mineral species containing Na, Mg, K, Ca, and Fe for OXY70 combustion of Utah Sufco 1 (Figure S3) (PDF)

■ AUTHOR INFORMATION

Corresponding Author

*E-mail: jost.wendt@utah.edu.

ORCID

Yueming Wang: 0000-0002-2059-4315

Jost O. L. Wendt: 0000-0002-0104-0763

Notes

The authors declare no competing financial interest.

■ ACKNOWLEDGMENTS

The authors acknowledge the financial support from the National Science Foundation (Award 1603249) that supported the bulk of the work reported here. Some results were also obtained under co-operative agreements from the Department of Energy (Awards DE-FE0025168 and DE-FE0029162). This work is also partially supported by the National Natural Science Foundation of China (Grant 51520105008).

■ REFERENCES

(1) Bryers, R. W. Fireside slagging, fouling, and high-temperature corrosion of heat-transfer surface due to impurities in steam-raising fuels. *Prog. Energy Combust. Sci.* **1996**, *22* (1), 29−120.

(2) Raask, E. *Mineral Impurities in Coal Combustion: Behavior, Problems, and Remedial Measures*; Hemisphere Publishing Corporation: New York, 1985.

(3) Baxter, L. L. *Ash Deposit Formation and Deposit Properties. A Comprehensive Summary of Research Conducted at Sandia's Combustion Research Facility*; Sandia National Laboratories: Livermore, CA, 2000; DOI: 10.2172/760515.

(4) Lighty, J. S.; Veranth, J. M.; Sarofim, A. F. Combustion aerosols: Factors governing their size and composition and implications to human health. *J. Air Waste Manage. Assoc.* **2000**, *50* (9), 1565−1618.

(5) Xu, M.; Yu, D.; Yao, H.; Liu, X.; Qiao, Y. Coal combustion-generated aerosols: Formation and properties. *Proc. Combust. Inst.* **2011**, *33* (1), 1681−1697.

(6) Nussbaumer, T. Combustion and co-combustion of biomass: Fundamentals, technologies, and primary measures for emission reduction. *Energy Fuels* **2003**, *17* (6), 1510−1521.

(7) Demirbas, A. Potential applications of renewable energy sources, biomass combustion problems in boiler power systems and combustion related environmental issues. *Prog. Energy Combust. Sci.* **2005**, *31* (2), 171−192.

(8) Koppejan, J.; Van Loo, S. *The Handbook of Biomass Combustion and Co-firing*; Routledge: Abingdon, U.K., 2012.

(9) Wendt, J. O. L.; Sternling, C. V.; Matovich, M. A. Reduction of sulfur trioxide and nitrogen oxides by secondary fuel injection. *Symp. (Int.) Combust., [Proc.]* **1973**, *14*, 897−904.

(10) Chen, L.; Yong, S. Z.; Ghoniem, A. F. Oxy-fuel combustion of pulverized coal: Characterization, fundamentals, stabilization and CFD modeling. *Prog. Energy Combust. Sci.* **2012**, *38* (2), 156−214.

(11) Kleinhans, U.; Wieland, C.; Frandsen, F. J.; Spliethoff, H. Ash formation and deposition in coal and biomass fired combustion systems: Progress and challenges in the field of ash particle sticking and rebound behavior. *Prog. Energy Combust. Sci.* **2018**, *68*, 65−168.

(12) Liu, C.; Liu, Z.; Zhang, T.; Huang, X.; Guo, J.; Zheng, C. Numerical Investigation on Development of Initial Ash Deposition Layer for a High-Alkali Coal. *Energy Fuels* **2017**, *31* (3), 2596−2606.

(13) Zhan, Z.; Bool, L. E.; Fry, A.; Fan, W.; Xu, M.; Yu, D.; Wendt, J. O. L. Novel temperature-controlled ash deposition probe system and its application to oxy-coal combustion with 50% Inlet O_2. *Energy Fuels* **2014**, *28* (1), 146−154.

(14) Babat, S.; Spörl, R.; Maier, J.; Scheffknecht, G. Investigation of deposit formation and its characterization for a pulverized bituminous coal power plant. *Fuel Process. Technol.* **2016**, *141*, 225−234.

(15) Zhan, Z.; Fry, A.; Wendt, J. O. L. Relationship between submicron ash aerosol characteristics and ash deposit compositions and formation rates during air-and oxy-coal combustion. *Fuel* **2016**, *181*, 1214−1223.

(16) Zhou, H.; Jensen, P. A.; Frandsen, F. J. Dynamic mechanistic model of superheater deposit growth and shedding in a biomass fired grate boiler. *Fuel* **2007**, *86* (10−11), 1519−1533.

(17) Lokare, S. S.; Dunaway, J. D.; Moulton, D.; Rogers, D.; Tree, D. R.; Baxter, L. L. Investigation of ash deposition rates for a suite of biomass fuels and fuel blends. *Energy Fuels* **2006**, *20* (3), 1008−1014.

(18) Lee, F.; Lockwood, F. Modelling ash deposition in pulverized coal-fired applications. *Prog. Energy Combust. Sci.* **1999**, *25* (2), 117−132.

(19) Shao, Y.; Wang, J.; Xu, C. C.; Zhu, J.; Preto, F.; Tourigny, G.; Badour, C.; Li, H. An experimental and modeling study of ash deposition behaviour for co-firing peat with lignite. *Appl. Energy* **2011**, *88* (8), 2635−2640.

(20) Rushdi, A.; Gupta, R.; Sharma, A.; Holcombe, D. Mechanistic prediction of ash deposition in a pilot-scale test facility. *Fuel* **2005**, *84* (10), 1246−1258.

(21) Fan, J.; Zha, X.; Sun, P.; Cen, K. Simulation of ash deposit in a pulverized coal-fired boiler. *Fuel* **2001**, *80* (5), 645−654.

(22) Wang, H.; Harb, J. N. Modeling of ash deposition in large-scale combustion facilities burning pulverized coal. *Prog. Energy Combust. Sci.* **1997**, *23* (3), 267−282.

(23) Richards, G. H.; Slater, P. N.; Harb, J. N. Simulation of ash deposit growth in a pulverized coal-fired pilot scale reactor. *Energy Fuels* **1993**, *7* (6), 774−781.

(24) Wessel, R. A.; Righi, J. Generalized correlations for inertial impaction of particles on a circular cylinder. *Aerosol Sci. Technol.* **1988**, *9* (1), 29−60.

(25) Zhou, M.-m.; Parra-Álvarez, J. C.; Smith, P. J.; Isaac, B. J.; Thornock, J. N.; Wang, Y.; Smith, S. T. Large-eddy simulation of ash deposition in a large-scale laboratory furnace. *Proc. Combust. Inst.* **2019**, *37*, 4409−4418.

(26) Brink, A.; Lindberg, D.; Hupa, M.; de Tejada, M. E.; Paneru, M.; Maier, J.; Scheffknecht, G.; Pranzitelli, A.; Pourkashanian, M. A temperature-history based model for the sticking probability of impacting pulverized coal ash particles. *Fuel Process. Technol.* **2016**, *141*, 210−215.

(27) Theis, M.; Skrifvars, B.-J.; Hupa, M.; Tran, H. Fouling tendency of ash resulting from burning mixtures of biofuels. Part 1: Deposition rates. *Fuel* **2006**, *85* (7−8), 1125−1130.

(28) Sami, M.; Annamalai, K.; Wooldridge, M. Co-firing of coal and biomass fuel blends. *Prog. Energy Combust. Sci.* **2001**, *27* (2), 171−214.

(29) Robinson, A. L.; Junker, H.; Baxter, L. L. Pilot-scale investigation of the influence of coal− biomass cofiring on ash deposition. *Energy Fuels* **2002**, *16* (2), 343−355.

(30) Abreu, P.; Casaca, C.; Costa, M. Ash deposition during the co-firing of bituminous coal with pine sawdust and olive stones in a laboratory furnace. *Fuel* **2010**, *89* (12), 4040−4048.

(31) Wang, G.; Pinto, T.; Costa, M. Investigation on ash deposit formation during the co-firing of coal with agricultural residues in a large-scale laboratory furnace. *Fuel* **2014**, *117*, 269−277.

(32) Fryda, L.; Sobrino, C.; Cieplik, M.; Van de Kamp, W. Study on ash deposition under oxyfuel combustion of coal/biomass blends. *Fuel* **2010**, *89* (8), 1889−1902.

(33) Lindner, E. R.; Wall, T. F. Sodium ash reactions during combustion of pulverised coal. *Symp. (Int.) Combust., [Proc.]* **1991**, *23*, 1313−1321.

(34) Neville, M.; Sarofim, A. The fate of sodium during pulverized coal combustion. *Fuel* **1985**, *64* (3), 384−390.

(35) Wibberley, L. J.; Wall, T. F. Alkali-ash reactions and deposit formation in pulverized-coal-fired boilers: Experimental aspects of sodium silicate formation and the formation of deposits. *Fuel* **1982**, *61* (1), 93−99.

(36) Paneru, M.; Babat, S.; Maier, J.; Scheffknecht, G. Role of potassium in deposit formation during wood pellets combustion. *Fuel Process. Technol.* **2016**, *141*, 266−275.

(37) Wang, C.; Li, G.; Du, Y.; Yan, Y.; Li, H.; Che, D. Ash deposition and sodium migration behaviors during combustion of Zhundong coals in a drop tube furnace. *J. Energy Inst.* **2018**, *91*, 251−261.

(38) Li, G.; Li, S.; Huang, Q.; Yao, Q. Fine particulate formation and ash deposition during pulverized coal combustion of high-sodium lignite in a down-fired furnace. *Fuel* **2015**, *143*, 430−437.

(39) Zhan, Z.; Fry, A.; Zhang, Y.; Wendt, J. O. L. Ash aerosol formation from oxy-coal combustion and its relation to ash deposit chemistry. *Proc. Combust. Inst.* **2015**, *35* (2), 2373−2380.

(40) Gallagher, N. B.; Peterson, T. W.; Wendt, J. O. L. Sodium partitioning in a pulverzed coal combustion environment. *Symp. (Int.) Combust., [Proc.]* **1996**, *26*, 3197−3204.

(41) Zhan, Z.; Wendt, J. O. L. Role of Sodium in Coal in Determining Deposition Rates. *Energy Fuels* **2017**, *31* (3), 2198−2202.

(42) Wang, Y.; Li, X.; Wendt, J. O. Ash aerosol and deposition formation mechanisms during air/oxy-combustion of rice husks in a 100 kW combustor. *Energy Fuels* **2018**, *32* (4), 4391−4398.

(43) Bonneville, A.; Gilmore, T.; Sullivan, C.; Vermeul, V.; Kelley, M.; White, S.; Appriou, D.; Bjornstad, B.; Gerst, J.; Gupta, N.; Horner, J.; McNeil, C.; Moody, M.; Rike, W.; Spane, F.; Thorne, P.; Zeller, E.; Zhang, F.; Hoffmann, J.; Humphreys, K. Evaluating the suitability for CO_2 storage at the FutureGen 2.0 site, Morgan County, Illinois, USA. *Energy Procedia* **2013**, *37*, 6125−6132.

(44) Zhan, Z.; Tian, S.; Fry, A.; Wendt, J. O. L. Formation of Ash Aerosols and Ash Deposits of Coal Blends. In *Clean Coal Technology and Sustainable Development*; Yue, G., Li, S., Eds.; Springer: Singapore, 2016; pp 121−131, DOI: 10.1007/978-981-10-2023-0_17.

(45) Murthy, B. N.; Sawarkar, A. N.; Deshmukh, N. A.; Mathew, T.; Joshi, J. B. Petroleum coke gasification: A review. *Can. J. Chem. Eng.* **2014**, *92* (3), 441−468.

(46) Zygarlicke, C.; Steadman, E.; Benson, S. Studies of transformations of inorganic constituents in a Texas lignite during combustion. *Prog. Energy Combust. Sci.* **1990**, *16* (4), 195−204.

(47) Zhan, Z.; Fry, A.; Yu, D.; Xu, M.; Wendt, J. O. L. Ash formation and deposition during oxy-coal combustion in a 100kW laboratory combustor with various flue gas recycle options. *Fuel Process. Technol.* **2016**, *141*, 249−257.

(48) Liu, H.; Wang, Y.; Wendt, J. O. L. Particle size distributions of fly ash arising from vaporized components of coal combustion—A comparison of theory and experiment. *Energy Fuels* **2018**, *32*, 4300−4307.

(49) Zhang, J.; Kelly, K. E.; Eddings, E. G.; Wendt, J. O. L. CO_2 effects on near field aerodynamic phenomena in 40kW, co-axial, oxy-coal, turbulent diffusion flames. *Int. J. Greenhouse Gas Control* **2011**, *5*, S47−S57.

DOI: 10.1021/acs.energyfuels.8b04185
Energy Fuels XXXX, XXX, XXX−XXX

(50) Morris, W.; Yu, D.; Wendt, J. O. L. Soot, unburned carbon and ultrafine particle emissions from air-and oxy-coal flames. *Proc. Combust. Inst.* **2011**, *33* (2), 3415−3421.
(51) Zhan, Z.; Fry, A.; Wendt, J. O. L. Deposition of coal ash on a vertical surface in a 100kW downflow laboratory combustor: A comparison of theory and experiment. *Proc. Combust. Inst.* **2017**, *36* (2), 2091−2101.

DOI: 10.1021/acs.energyfuels.8b04185
Energy Fuels XXXX, XXX, XXX−XXX